J Theor Appl Phys (2016) 10:233–240
DOI 10.1007/s40094-016-0221-0

RESEARCH

Synthesis, structural and optical properties of pure ZnO and Co doped ZnO nanoparticles prepared by the co-precipitation method

P. Geetha Devi[1] · A. Sakthi Velu[2]

Received: 11 November 2015 / Accepted: 20 April 2016 / Published online: 7 May 2016

Abstract Pure ZnO and Cobalt (Co) doped ZnO nanoparticles (NPs) were synthesized by the co-precipitation method. The synthesized nanoparticles retained the wurtzite hexagonal structure, which was confirmed by X-ray diffraction studies. From FESEM studies, ZnO and Co doped ZnO NPs showed Spherical and nanorod mixed phase and Spherical like morphology, respectively. The amount of dopant (Co^{2+}) incorporated into ZnO sample was determined by EDAX. The FT-IR spectra confirmed the Zn–O stretching bands at 438 and 427 cm^{-1} for ZnO and Co doped ZnO NPs. From the UV–VIS spectroscopic measurements, the excitonic pecks were found around 376 and 370 nm for the respective samples. The photoluminescence measurements revealed that the broad emission was composed of seven different bands due to zinc vacancies, oxygen vacancies and surface defects. The dynamic light scattering (DLS) and Zeta potential measurements were used to find out the size and surface charges.

Keywords Co-precipitation · ZnO NPs · Photoluminescence · DLS and Zeta potential

Introduction

The ZnO is a semiconductor with a wide band gap (3.37 eV), large exciton binding energy (60 meV), n-type conductivity, abundant in nature and environmentally friendly. These characteristics make this material attractive for many applications, such as solar cells, optical coatings, photo catalysts, electrical devices, active medium in UV semiconductor lasers and in gas sensors [1, 2]. The synthesis of size and shape-controlled metal oxide nanostructures is very important in controlling their physical and chemical properties for their potential applications. The optical properties of nanocrystalline semiconductors have been studied extensively in recent years. As the size of the material becomes smaller and the band gap becomes larger, this changes the optical and electrical properties of the material, making it suitable for new applications and devices. Among them, the widely accepted method to modify the electrical and optical properties of a semiconductor is the addition of impurity atoms, or doping [3–5]. The different type of shapes, such as nanorods, tetrapods and nanowire [6] formed by adding dopants insulating material begun to work as semiconductors and such semiconducting nanomaterials can be used for wavelength-tunable lasers [7], bio-imaging [8] and solar cells [9]. There are several methods reported in the literature for the synthesis of undoped, doped ZnO NPs and its derivatives which can be categorized into either (Chemical or Physical, co-precipitation, hydrothermal, solvothermal, emulsion and microemulsion methods etc.) [10–28]. Among the various methods, co-precipitation is one of the most important methods to prepare the nanoparticles. Recently, it has been reported that, Cobalt doped ZnO nanoparticles photoluminescence intensity owing to the vacancies varies with the Co concentration because of the increment of oxygen vacancies [29]. Nair et al. (2011) report suggest that ZnO:Co^{2+} nanoparticles can be used as immobilized photo catalysts for water and environmental detoxification from organic compounds, inorganic compounds like arsenic and bacteria [30].

✉ P. Geetha Devi
nanophd15@gmail.com

[1] Department of Physics, M.A.M. College of Engineering, Siruganur, Tiruchirappalli 621105, TN, India

[2] PG and Research Department of Physics, Periyar E.V.R. College (Autonomous), Tiruchirappalli 620023, TN, India

In the present investigation, pure and Co-doped ZnO NPs are synthesized by the co-precipitation method. We have studied the structural and optical properties of the pure and Co-doped ZnO NPs.

Experimental sections

Preparation of the pure and Co doped ZnO NPs

The following high purity chemicals, such as Zinc (II) nitrate hexahydrate $Zn(NO_3)_2{\cdot}6H_2O$, Cobalt nitrate hexahydrate $Co(NO_3)_2{\cdot}6H_2O$, Sodium hydroxide NaOH and Poly ethylene glycol (PEG) were used as the precursors without further purification. The experimental procedure for the preparation of pure ZnO and transition metal (Co)doped ZnO samples is as follows: For the preparation of pure ZnO NPs, 0.1 M of Zinc Nitrate hexahydrate, 0.8 M of NaOH and 5.0 g of PEG were separately dissolved in each 100 ml of distilled water using three 200 ml beakers. At first, Zinc Nitrate and PEG solutions were mixed homogenously. Next, NaOH solution was added drop wise to the homogenous mixed solution, yielding a white precipitate. The solution with the white precipitate was stirred at the room temperature for 30 min, and then at temperature of 60 °C for 4 h. This solution was refluxed at room temperature for 24 h. Then, a clear solution was obtained, which found to be stable at ambient condition. Thereafter, the solution was washed several times with double distilled water and ethanol. Finally, the precipitate was dried at 120 °C. Thus, ZnO nanopowder was obtained. Similarly, for the preparation of Co-doped ZnO NPs, in case of the Co-doped sample, 0.005 M of aqueous Cobalt nitrate hexahydrate solution was added into 0.095 M of aqueous Zinc Nitrate solution. This solution was mixed into 100 ml of an aqueous solution containing 5.0 g of PEG. 0.8 M of aqueous NaOH solution was added drop wise to this homogenous mixture to form a white precipitate. The solution with the white precipitate was processed as above to obtain Co-doped ZnO sample. Thus, pure ZnO and transition metal-doped ZnO samples were obtained. These samples were annealed at 600 °C for 4 h because the energy from the heat could enhance the vibration and diffusion of lattice atoms for atomic for crystallization.

Characterization

The ZnO and Co doped ZnO NPs were characterized by X-ray diffractometer (model: X'PERT PRO PANalytical). The diffraction patterns were recorded in the range of 20°–80° for the ZnO samples where the monochromatic wavelength of 1.5405 Å was used. The samples were analyzed by FESEM (model: SUPRA 55) with EDAX (model: ULTRA 55). The FT-IR spectra were recorded in the range of 400–4000 cm^{-1} by using Perkin Elmer spectrometer. The UV–VIS spectra were recorded in the wavelength range 190–1110 nm by using Lambda 35 UV–VIS spectrophotometer. Room temperature PL measurements were performed for pure ZnO and Co doped ZnO NPs samples with excitation wavelength of 325 nm using Perkin Elmer spectra fluorometer. The emission spectra were recorded in the UV and visible range (330–600 nm).

Results and discussion

X-ray diffraction studies

The X-ray diffraction peaks of pure ZnO and Co doped ZnO NPs are shown in Fig. 1a. The pronounced diffraction peaks are clearly exhibiting the crystalline nature with peaks corresponding to (100), (002), (101), (102), (110), (103), (200), (112) and (201) planes. The standard diffraction peaks reveal that the crystal structure of ZnO and Co doped ZnO NPs is of hexagonal wurtzite structure (space group p63mc, JCPDS data card no: 79-2205). The compared pure ZnO and JCPDS data values are given in the Table 1. Interestingly, the Co doped ZnO NPs sample showed no additional phase formation. To examine the effect of Co doping on structure, an enlarged version of the XRD pattern between 35.8° and 37° is shown in Fig. 1b. It is worthy to mention that there is slight higher angle shift compared to pure ZnO NPs, suggesting that Co has been doped in ZnO in accordance with Vegard's law. Since the ionic radii of Zn^{2+} and Co^{2+} are 0.0740 and 0.065 nm, respectively, the replacement of Co^{2+} into Zn^{2+} sites makes the variation in '*d*' values. The lattice constants '*a*' and '*c*' of wurtzite structure can be calculated by using the relation

$$\frac{1}{d^2} = \frac{4}{3}\left(\frac{h^2 + hk + k^2}{a^2}\right) + \frac{l^2}{c^2} \tag{1}$$

with the first order approximation ($n = 1$),

$$\sin^2\theta = \frac{\lambda^2}{4}\left(\frac{4}{3}\left(\frac{h^2 + hk + k^2}{a^2}\right) + \frac{l^2}{c^2}\right) \tag{2}$$

for (100) orientation at $2\theta \approx 31.764°$ and 31.865° for pure ZnO and Co doped ZnO NPs, respectively, the lattice constant *a* is calculated by

$$a = \frac{\lambda}{\sqrt{3}sin\theta} \tag{3}$$

For (002) orientation at $2\theta \approx 34.412°$ and 34.517° for pure ZnO and Co doped ZnO NPs, respectively, the lattice constant c is calculated by

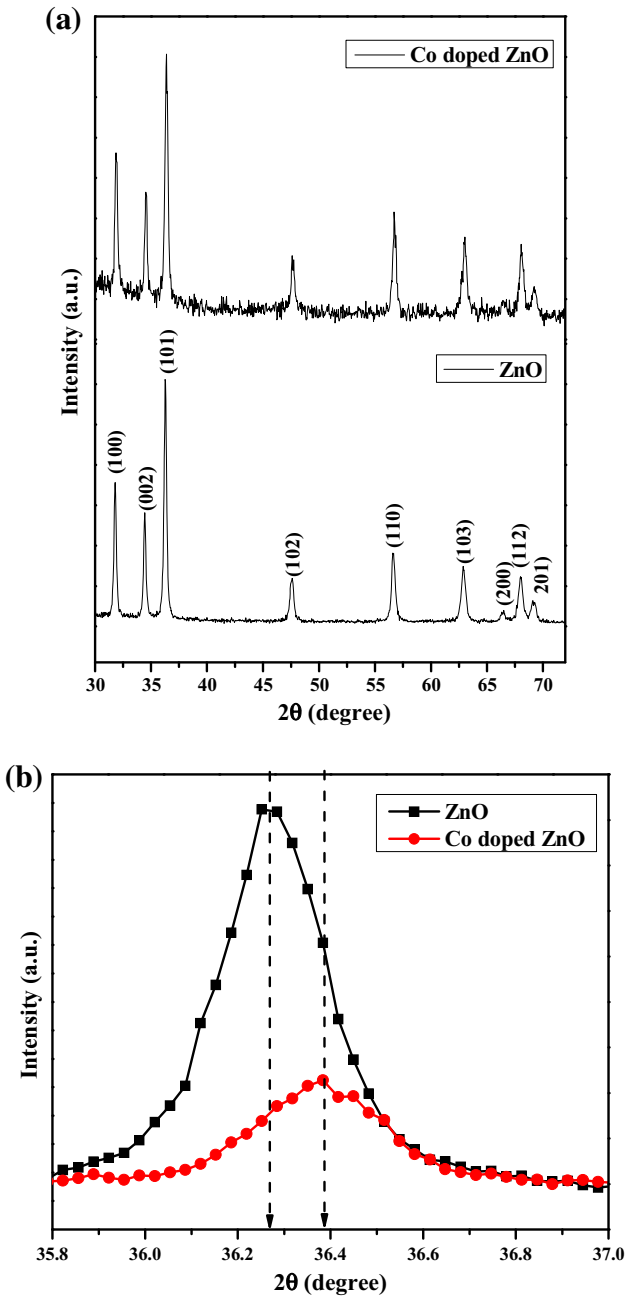

Fig. 1 X-ray powder diffraction pattern of (**a**) pure ZnO and Co doped ZnO NPs and (**b**) an enlarged version of the XRD pattern between 35.8° and 37°

$$c = \frac{\lambda}{sin\theta} \tag{4}$$

The lattice constant '*a*' values are calculated as 3.2503 and 3.2405 Å and '*c*' values are 5.2081 and 5.1928 Å for pure ZnO and Co doped ZnO NPs, respectively. The change in the lattice parameter values can be ascribed by the substitution of Co^{2+} ion in Zn^{2+} sites, which has a higher ionic radius than Zn^{2+} in their tetrahedral coordinates. The unit cell volumes decrease with the doping of Co^{2+} ions. The values are 47.6479 and 47.2160 $Å^3$ for pure ZnO and Co doped ZnO NPs, respectively. This indicates that these Co ions reside partially in tetrahedral Zn lattice sites.

As compared to the pure ZnO NPs, the intensity of XRD peaks decreases and FWHM increases in the case of Co doped ZnO NPs due to the degradation of crystallinity. The values are given in Table 2. The variation in the values reveals that even through the Co ions occupy the regular lattice site of ZnO, it produces crystal defects around the dopants and these defects change the stoichiometry of the materials. The bond length (*L*) of Zn–O is calculated by using relation [31] $L = \sqrt{\left(\frac{a^2}{3} + \left(\frac{1}{2} - u\right)^2 c^2\right.}$ where '*a*' and '*c*' are lattice parameters and '*u*' is positional parameter which is a measure of the amount by which each atom is displaced with respect to the next along the '*c*' axis. The parameter '*u*' can be calculated by the formula $u = \left(\frac{a^2}{3c^2}\right) + 0.25$. There is a strong correlation between the *c*/*a* ratio and '*u*'. The *c*/*a* ratio decreases with increasing '*u*' in such a way that those four tetrahedral distances remain nearly constant through a distortion of tetrahedral angels due to the long-range polar interaction. In our study, the *c*/*a* ratio increase in the Co doped ZnO NPs compared to that of the pure ZnO NPs (Table 2). The bond length of Zn–O is found to be 1.9781 and 1.9722 Å for pure ZnO NPs and Co doped ZnO NPs, respectively.

This change in bond lengths is attributed to higher ionic radius of Co^{2+}. In hexagonal wurtzite structure where the metal and oxygen ion (for ZnO) face directly in '*c*' axis, but for the '*a*' and '*b*' axis, the structure contains only oxygen ions facing each other. The oxygen ion diagonally connects the metal ions. This is the reason that the variation is significant in '*c*' axis but not in '*a*' axis [32].

The average crystallite size (*D*) of the NPs is calculated after appropriated background corrections from X-ray line broadening of the diffraction peaks using Debye–Scherrer's formula.

$$D = \frac{0.9\lambda}{\beta cos\theta} \tag{5}$$

where λ is the wavelength of X-ray used (1.5405 Å), β is the angular peak width at half maximum in radians and θ is Bragg's diffraction angle. The average particle size is calculated as 35 and 28 nm for pure ZnO and Co doped ZnO NPs, respectively. The reduction in the particle size is mainly due to the distortion in the host ZnO lattice by the foreign impurity i.e., Co^{2+}.

Field emission scanning electron microscopic analyzes

The FESEM images of the pure ZnO and Co-doped ZnO NPs are shown in Fig. 2a, b. From the images, we can see

Table 1 As compared ZnO NPs and JCPDS data values

JCPDS card no: (79-2205) 2θ (degree)	ZnO 2θ (degree)	ZnO:Co 2θ (degree)	JCPDS card no: (79-2205) d-spacing (Å)	ZnO d-spacing (Å)	ZnO:Co d-spacing (Å)	ZnO FWHM β (°)	ZnO:Co FWHM β (°)	(hkl)	JCPDS card no: (79-2205) relative intensity	ZnO relative intensity	ZnO:Co relative intensity
31.79	31.76	31.86	2.81	2.81	2.80	0.22	0.25	100	56.40	54.34	60.08
34.41	34.41	34.51	2.60	2.60	2.59	0.21	0.22	002	41.50	43.61	48.16
36.25	36.24	36.34	2.47	2.47	2.46	0.23	0.29	101	99.99	100.00	100.00
47.53	47.53	47.63	1.91	1.91	1.90	0.35	0.24	102	21.10	17.84	24.85
56.59	56.59	56.69	1.62	1.62	1.62	0.29	0.31	110	30.50	31.68	42.22
62.85	62.85	62.96	1.47	1.47	1.47	0.42	0.31	103	26.80	20.97	32.46
66.37	66.36	66.43	1.40	1.40	1.40	0.40	0.30	200	4.00	4.33	4.53
67.94	67.96	68.04	1.37	1.37	1.37	0.36	0.39	112	21.70	15.65	32.08
69.08	69.12	69.17	1.35	1.35	1.35	0.42	0.50	201	10.60	7.15	13.80
76.95	76.94	77.00	1.23	1.23	1.23	0.70	0.50	202	3.30	2.71	2.87

Table 2 X-ray diffraction parameter values of the pure ZnO and Co-doped ZnO NPs

Sample	Lattice parameter values (Å)		Atomic packing factor (c/a)	Volume V (Å)^3	Cos φ	Position parameter (u)	Bond length Zn–O L (Å)	Average crystalline size D (nm)	Micro-strain ε
	a	c							
ZnO	3.2503	5.2081	1.6023	47.6479	0.84739	0.37980	1.9781	35.277	0.00252
ZnO:Co	3.2405	5.1928	1.6025	47.2160	0.84739	0.37979	1.9722	28.883	0.00167

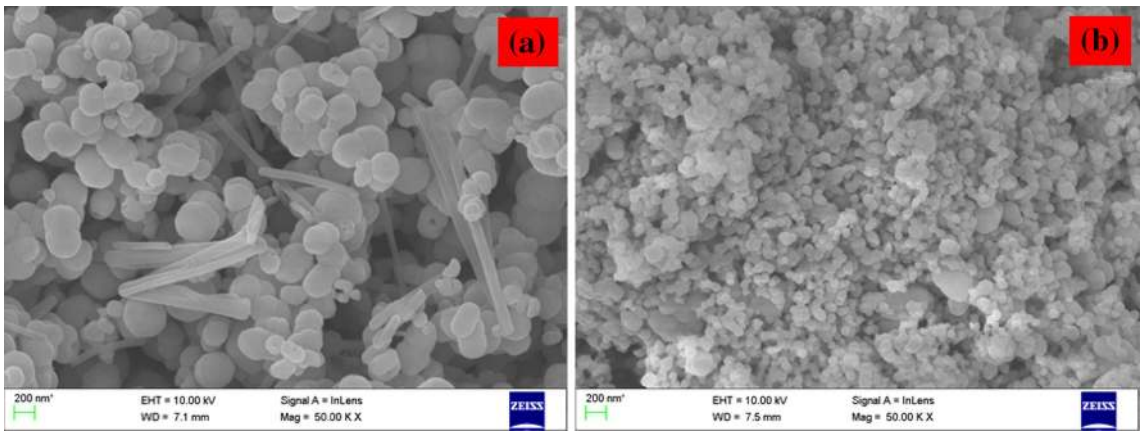

Fig. 2 FESEM image of (**a**) pure ZnO, and (**b**) Co doped ZnO NPs

that the pure ZnO nanoparticles are found to be spherical and rod like mixed phase but the Co doped ZnO form spherical structure formed. The particles sizes are found to be 74 and 52 nm for pure ZnO and Co doped ZnO NPs, respectively. The particles sizes of the Co doped ZnO NPs are found to be reduced as compared to that of pure ZnO NPs. This reduction in particles size is due to the distortion in the host material incorporated with Co^{2+} metal ion in ZnO NPs surface area. Hence the sizes of ZnO NPs are reduced by Co doping.

Energy dispersive analysis X-ray (EDAX) studies

The compositional analysis of the pure ZnO and Co doped ZnO samples were carried out using EDAX. The typical EDAX spectra of the pure ZnO, Co doped ZnO samples are

shown in Fig. 3a, b. From the EDAX analysis, the amounts of transition metal ion present in the doped ZnO NPs as shown in Fig. 3a, b. In the doped samples, the concentrations of Co are found to be 3.83 %, respectively. In the pure ZnO Samples, the chemical compositions of Zn and O are found to be 56.42 and 43.58 %, respectively. However, for the Co doped ZnO samples, the Zinc percentage decrease whereas the oxygen percentage increase.

FT-IR spectroscopic studies

The FT-IR spectra of the prepared ZnO and Co doped ZnO NPs are shown in Fig. 4. The FT-IR measurements are performed for the samples using the KBr pallet method in the wave number range 400–4000 cm^{-1}. The broad absorption in the frequency band 3750–3000 cm^{-1} is assigned to O–H stretching from residual alcohols, water and Zn–OH [33]. The absorption peaks are observed at 3442 and 3421 cm^{-1} for the ZnO and Co doped ZnO NPs samples, respectively. The H-OH bending mode origin is at 1549 and 1540 cm^{-1} for ZnO and Co doped ZnO NPs samples, respectively. The bands are observed at 881 and 880 cm^{-1} due to the C-H out-of plane bending of the polyethylene glycol group for the pure ZnO, and Co doped ZnO NPs samples. The most intense broad absorption band at $\sim$438 cm^{-1} is attributed to the stretching of vibration of ZnO [34]. The Zn-O stretching bands are observed at 438 and 427 cm^{-1} for the respective pure ZnO and Co doped ZnO NPs samples.

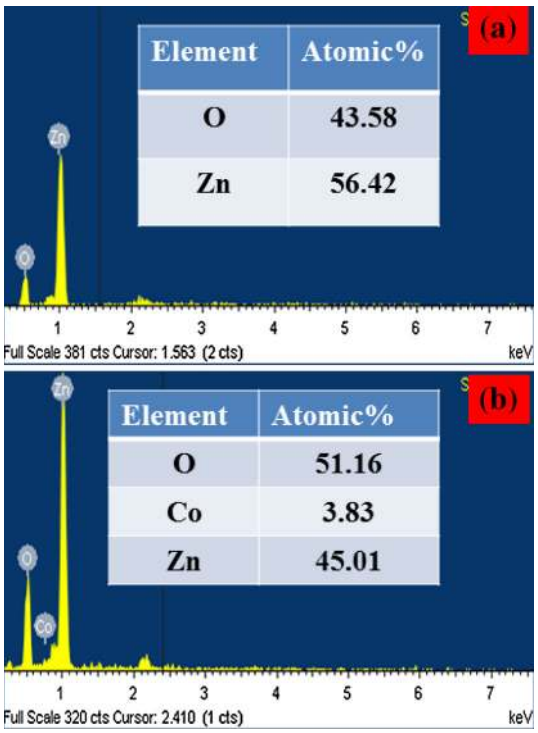

Fig. 3 EDAX spectra of (**a**) pure ZnO, and (**b**) Co doped ZnO NPs

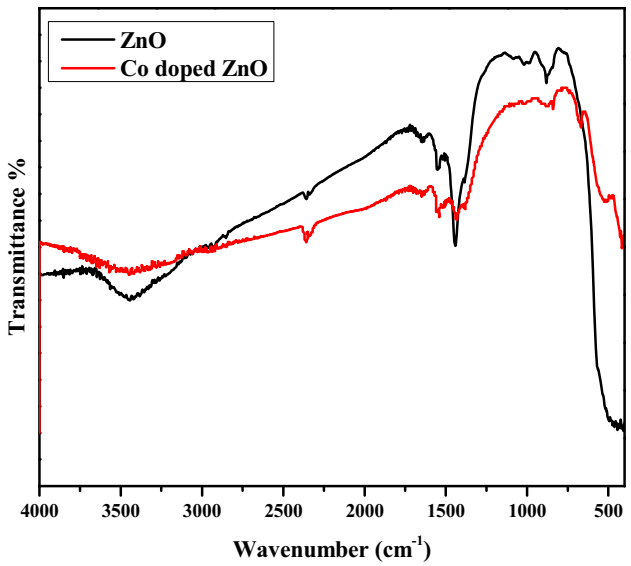

Fig. 4 FT-IR absorption spectra of (**a**) ZnO NPs and (**b**) Co doped ZnO NPs

UV–VIS–NIR spectroscopic studies

The absorbance of the samples is depended on several factors, such as band gap, oxygen deficiency, surface roughness and impurity centers. The excitonic pecks are observed around 376 and 370 nm for the ZnO and Co doped ZnO NPs, respectively. The optical energy band gap of undoped and Co doped ZnO NPs is calculated by classical Tauc relation as given below.

$$\alpha h\upsilon = A\left(h\upsilon - E_g\right)^n$$

where E_g is the optical bandgap. A is a constant and the exponent n depends on the transition. The value of ($n = 1/2$, 3/2, 2, or 3) depends on the nature of the electronic transition (1/2 for allowed direct transition, 2 for allowed in-direct transition, 3/2 and 3 for forbidden direct and forbidden indirect transition, respectively). Considering direct band transition in ZnO, a plot between $(\alpha h\upsilon)^2$ versus photon energy ($h\upsilon$) is drawn for ZnO and Co doped ZnO NPs and is shown in Fig. 5a, b. Extrapolation of linear region of these plots to $(\alpha h\upsilon)^2 = 0$ gives the corresponding direct energy band gap. The band gap of 3.30 and 3.35 eV is obtained for ZnO and Co doped ZnO NPs, respectively. Comparing it with that of the pure ZnO NPs, the increase in the band gap or blue shift can be explained on the basis of the Burstein-Moss effect [35], while the Fermi level shifts close to the conduction band due to the increase in the carrier concentration the low energy transition are blocked and the value of band gap increase due to the incorporation of Co^{2+} ion in ZnO lattice.

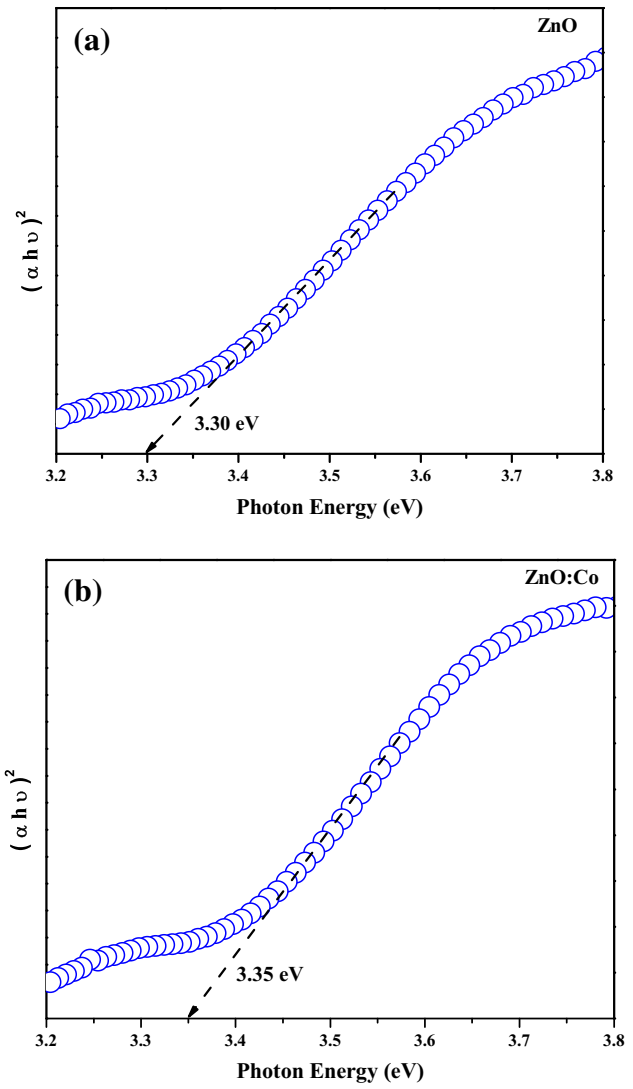

Fig. 5 Band gap measurement for $n = 1$ excitonic state of (**a**) ZnO NPs and (**b**) Co doped ZnO NPs

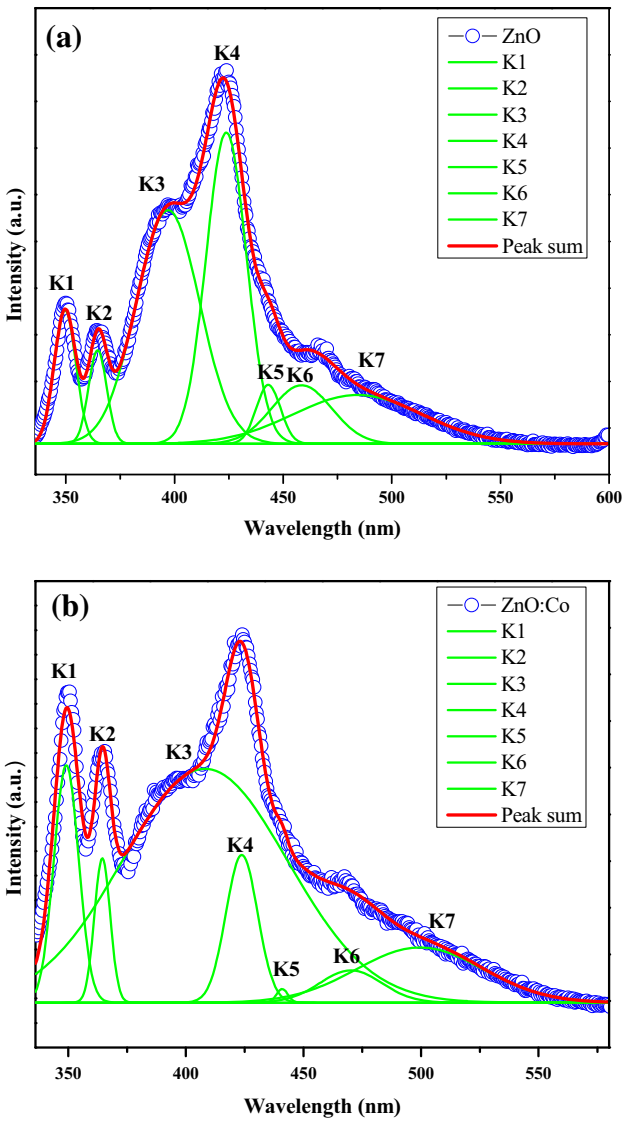

Fig. 6 Gaussian de-composed photoluminescence emission spectra of (**a**) Pure ZnO NPs and (**b**) Co doped ZnO NPs

Photoluminescence studies

The photoluminescence spectrum of the pure ZnO and Co doped ZnO is shown in Fig. 6a, b. The photoluminescence spectra of the pure ZnO and Co doped ZnO NPs samples recorded with the excited wavelength of 325 nm. The PL emission is observed for ZnO samples covering from the very short wavelength of 340 nm to long wavelength 575 nm. A good fit of seven peaks Gaussian function is obtained for all the PL spectra of the samples at the bottom labeled as K1, K2, K3, K4, K5, K6 and K7. The solid lines represent the linear combination of five Gaussian peaks K1 has the lowest and K7 has the highest wavelength.

The emission spectra of the ZnO NPs sample having seven peaks at 349, 364, 397, 423, 443, 458 and 484 nm. These bands are three Near Band Edge emission, Violet emission, two blue emission and blue-green emission, respectively. The NBE emissions K1, K2 and K3 is located at UV region (349, 364 and 397 nm) for pure ZnO NPs, this NBE emission is attributed to the radiative recombination between the electrons in the conduction band and the holes in the valence band. The K4 peak is the origin of the violet emission centered at 423 nm, and is ascribed to an electron transition from a shallow donor level of the natural zinc interstitials to the top level of the valence band [35]. The two blue emission band (K5 and K6) at 443 and 458 nm is attributed to singly ionized Zn vacancies [36]. There are blue-green emission bands (K8) at 484 nm due to a surface defects in the ZnO NPs corresponding to the transition between oxygen vacancy and oxygen interstitial defect [37].

The values of emission bands K1, K2, K3, K4, K5, K6 and K7 of the Co-doped ZnO NPs values are 349, 364, 408, 423, 440, 470 and 499 nm, respectively. As compared to pure ZnO NPs, the red shift is observed for the Co doped ZnO NPs. The red shift may be from different origins, such as electron phonon coupling, lattice distortion, localization of charge carriers due to interface effects and point defects. For the Co doped ZnO NPs, the changes in the emission values confirm the substitution of Co^{2+} into the ZnO lattice sites.

Dynamics light scattering studies

The dynamic light scattering (DLS) were used to find out the size and surface charges of nanoparticles. From Fig. 7a, b chemically synthesized ZnO and Co doped ZnO NPs average particle size distribution were 344 and 141 nm, respectively. The same result conformed in XRD patterns. The Zeta potential analysis revealed the surface charge of ZnO and Co doped ZnO NPs to be 12.1 and −4.43 mV as shown in Fig. 8a, b.

In summary, Co-doped ZnO NPs were prepared through the co-precipitation method. The X-ray diffraction study confirmed that the prepared particles were of the hexagonal wurtzite structure. From the FESEM images, the particles were found to exhibit, the pure ZnO NPs sample formed spherical and rod like morphology and the Co doped ZnO formed spherical like morphology, respectively. Co doped ZnO NPs particles size reduced as compare to pure ZnO NPs. From the EDAX analysis, the chemical compositions were estimated for the prepared samples. Using the recorded FT-IR spectra, the various vibrational frequencies were assigned for the pure ZnO and Co-doped ZnO samples. The photoluminescence studies showed that the doping of ZnO altered the band emission, which is due to zinc vacancies, oxygen vacancies and surface defects. The antibacterial efficiency of ZnO NPs generally depends on the presence of more ROS, which was mainly attributed to the increase in oxygen vacancies. The ZnO NPs as compare to the Co-doped ZnO NPs oxygen vacancies were increased. The dynamic light scattering (DLS) and Zeta potential were used to find out the size and surface charges. So that Co-doped ZnO NPs were used for antibacterial applications.

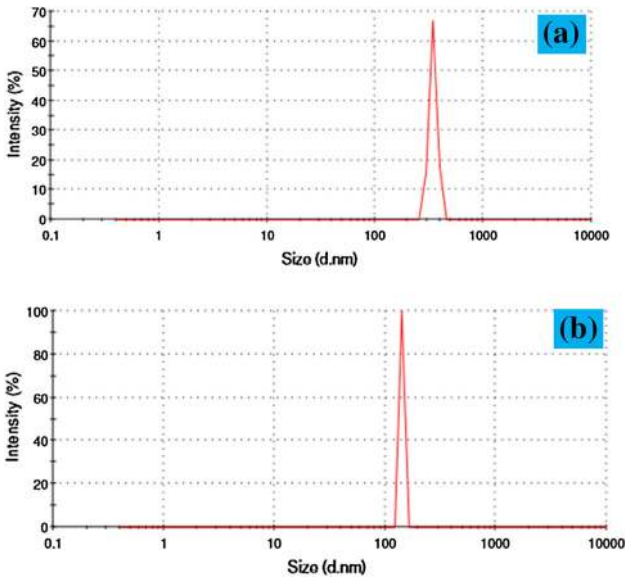

Fig. 7 DLS spectra of (**a**) Pure ZnO NPs and (**b**) Co doped ZnO NPs

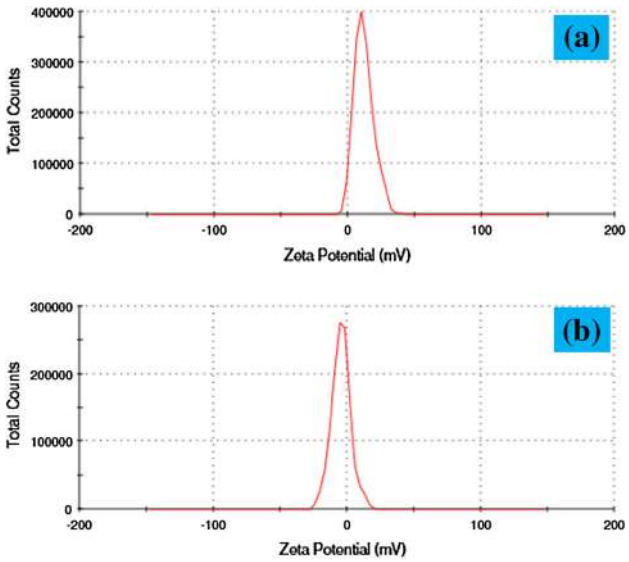

Fig. 8 Zeta potential measurements of (**a**) Pure ZnO NPs and (**b**) Co doped ZnO NPs

References

1. Pivin, J.C., Socol, G., Mihailescu, I., Berthet, P., Singh, F., Patel, M.K.: Thin Solid Films **517**, 916–922 (2008)
2. Sato, K., Yoshida, H.K.: Jpn. J. Appl. Phys. **39**, L555–L558 (2000)
3. Hsu, L.S., Yeh, C.S., Kuo, C.C., Huang, B.R., Dhar, S.: J. Optoelectron. Adv. Mater. **7**, 3039–3046 (2005)
4. Bhargava, R.N., Haranath, D., Metha, A.: J. Korean Phys. Soc. **53**, 2847–2851 (2008)
5. Bae, S.Y., Na, C.W., Kang, J.H., Park, J.: J. Phys. Chem. B **109**, 2526–2531 (2005)
6. Yin, Y., Alivisators, A.P.: Nature **437**, 664 (2005)
7. Kilmov, V.I., Ivaov, S.A., Nanda, J., Achermann, M., Bezel, I., McGuire, J.A., Piryatinski, A.: Nature **447**, 664 (2005)

8. Michalet, X., Pinaud, F.F., Bentolila, L.A., Tsay, J.M., Doose, S., Li, J.J., Sundaresan, G., Wu, A.M., Gambhir, S.S., Weiss, S.: Science **307**, 538 (2005)
9. Gur, I., Fromer, N.A., Geier, M.L., Alivisatos, A.P.: Science **310**, 462 (2005)
10. Djerdj, I., Jaqlicic, Z., Arcon, D., NiederBerger, M.: Nanoscale **2**, 1096–1104 (2010)
11. Djerdj, I., Garnweitner, G., Arcon, D., Pregeli, M., Jaqlicic, Z., Niederberger, M.: J. Mater. Chem. **18**, 5208–5217 (2008)
12. Hirano, S.I.: Am. Ceram. Soc. Bull. **66**, 1342–1344 (1987)
13. Vorkapic, D., Matsoukas, T.: J. Am. Chem. Soc. **81**, 2815–2820 (1998)
14. Haja Hameed, A.S., Karthikeyan, C., Sasikumar, S., Senthil Kumar, V., Kumaresan, S., Ravi, G.: J. Mater. Chem. B **1**, 5950–5962 (2013)
15. Radzimska, A.K., Jesionowski, T.: Materials **7**, 2833–2881 (2014)
16. Radzimska, A.K., Jesionowski, T., Krysztafkiewicz, A.: Physicochem. Probl. Miner. Process. **44**, 93–102 (2010)
17. Hong, R., Pan, T., Qian, J., Li, H.: Chem. Eng. J. **119**, 331–335 (2006)
18. Lanje, A.S., Sharma, S.J., Ningthoujam, R.S., Ahn, J.S., Pode, R.B.: Adv. Powder Technol. **24**, 331–335 (2013)
19. Wang, Y., Zhang, C., Bi, S., Luo, G.: Powder Technol. **202**, 130–136 (2010)
20. Cao, Z., Zhang, Z., Wang, F., Wang, G.: Colloids Surf. A Physicochem. Eng. Asp. **340**, 161–167 (2009)
21. Khoshhesab, Z.M., Sarfaraz, M., Houshyar, Z.: Synth. React. Inorg. Met. Org. Nano Met. Chem. **42**, 1363–1368 (2012)
22. Kumra, K.M., Mandal, B.K., Naidu, E.A., Sinha, M., Kumar, K.S., Reddy, P.S.: Spectrochim. Acta Part A Mol. Biomol. Spectrosc. **104**, 171–174 (2013)
23. Wang, Y., Ma, C., Sun, X., Li, H.: Inorg. Chem. Commun. **5**, 751–755 (2002)
24. Benhebal, H., Chaib, M., Salomon, T., Geens, J., Leonard, A., Lambert, S.D., Crine, M., Heinrichs, B.: Alex. Eng. J. **52**, 517–523 (2013)
25. Yue, S., Yan, Z., Shi, Y., Ran, G.: Mater. Lett. **98**, 246–249 (2013)
26. Chen, D., Ciao, X., Cheng, G.: Solid State Commun. **113**, 363–366 (2000)
27. Wysokowski, M., Motylenko, M., Stocker, H., Bazhenov, V.V., Langer, E., Dobrowolska, A., Czaczyk, K., Galli, R., Stelling, A.L., Behm, T., Klapiszewski, L., Ambrożewicz, D., Nowacka, M., Molodtsov, S.L., Abendroth, B., Meyer, D.C., Kurzydłowski, K.J., Jesionowski, T., Ehrlich, H.: J. Mater. Chem. B **1**, 6469 (2013)
28. Geetha Devi, P., Sakthi Velu, A.: J. Adv. Appl. Sci. Res. **2**, 130–137 (2015)
29. Sharma, P.K., Dutta, R.K., Pandey, A.C.: J. Colloid Interf. Sci. **345**, 149–153 (2010)
30. Nair, M.G., Nirmala, M., Rekha, K., Anukaliani, A.: Mater. Lett. **65**, 1797–1800 (2011)
31. Wang, X.S., Wu, Z.C., Webb, J.F., Liu, Z.G.: Appl. Phys. A Mater. Sci. Process. **77**, 561–565 (2003)
32. Karthikeyan, B., Pandiyarajarn, T., Mangaiyarkarasi, K.: Spectrochim. Acta Part A **82**, 97–101 (2011)
33. Senthilkumaar, S., Rajendran, K., Banerjee, S., Chini, T.K., Sengodan, V.: Mater. Sci. Semi. Process **11**, 6–12 (2008)
34. Xiong, G., Pal, U., Serrano, J.G.: J. Appl. Phys. **101**, 24317 (2007)
35. Suwanboon, S., Ratana, T., Ratana, W.T.: J. Sci. Technol. **4**, 111–121 (2007)
36. Fan, X.M., Lian, J.S., Zhao, L., Liu, Y.H.: Appl. Surf. Sci. **252**, 420–424 (2005)
37. Mishra, S.K., Srivastava, R.K., Prakash, S.G., Yadav, R.S., Panday, A.C.: Opto Electron. Rev. **18**, 467–473 (2010)